Catalysis Science & Technology

Accepted Manuscript

ROYAL SOCIETY OF CHEMISTRY

www.rsc.org/catalysis

Magnetically Separable Reduced Graphene Oxide/Iron Oxide Nanocomposite Materials for Environmental Remediation

Teo Peik-See, Alagarsamy Pandikumar, Lim Hong Ngee,

Huang Nay Ming, Chia Chin Hua

Graphical Abstract

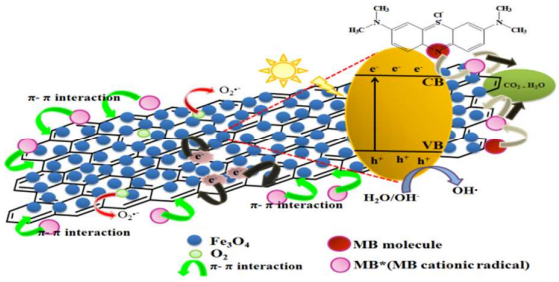

Synthesis of magnetically separable rGO/Fe_3O_4 nanocomposite materials for environmental remediation *via* photocatalytic degradation of methylene blue.

Magnetically Separable Reduced Graphene Oxide/Iron Oxide Nanocomposite Materials for Environmental Remediation

Teo Peik-See[1], Alagarsamy Pandikumar[1*], Lim Hong Ngee[2,3], Huang Nay Ming[1*], Chia Chin Hua[4]

[1]Department of Physics, Faculty of Science, University of Malaya, 50603 Kuala Lumpur, Malaysia

[2]Department of Chemistry, Faculty of Science, Universiti Putra Malaysia, 43400 UPM Serdang, Selangor, Malaysia

[3]Functional Device Laboratory, Institute of Advanced Technology, Universiti Putra Malaysia, 43400 UPM Serdang, Selangor, Malaysia

[4]School of Applied Physics, Faculty of Science and Technology, Universiti Kebangsaan Malaysia, 43600 Bangi, Selangor, Malaysia

*Corresponding author(s): pandikumarinbox@gmail.com and huangnayming@um.edu.my

Tel: +6-0163301609.

Abstract

Magnetically separable reduced graphene oxide/iron oxide (rGO/Fe_3O_4) nanocomposite materials were synthesized at room temperature through a facile, eco-friendly and cost-effective approach. The prepared nanocomposite materials were characterized by different techniques. The x-ray diffraction analysis revealed the formation of rGO/Fe_3O_4 nanocomposites, while the transmission electron microscopic images showed that the Fe_3O_4 nanoparticles with an average size of 10 nm were embedded uniformly on the surface of rGO sheets. The synthesized rGO/Fe_3O_4 nanocomposite materials were found to be super-paramagnetic in nature at room temperature. The photocatalytic performance of the rGO/Fe_3O_4 nanocomposite materials was investigated under natural sunlight irradiation by employing methylene blue (MB) as a model target organic pollutant. The rGO/Fe_3O_4 showed better adsorption behaviour and excellent photocatalytic activity towards the degradation of MB. This enhanced photocatalytic activity could be attributed to the synergistic effect that arises between the rGO and Fe_3O_4 which significantly reduces the charge recombination. Moreover, the rGO/Fe_3O_4 nanocomposite materials exhibited good sustainability, which was disclosed by their constant photocatalytic performance and the absence of any observable changes in the morphology even after eight cycles of operation during photocatalytic experiments. The overall results of the study indicate that this newly prepared photocatalytically stable and magnetically separable rGO/Fe_3O_4 nanocomposite could be potentially utilized for many environmental remediation applications.

Keywords: Nanocomposite; Reduced graphene oxide; Magnetically separable photocatalyts; Waste water treatment.

1. Introduction

The requirement of fresh water is most essential for all living organisms including human beings and such availability is a foremost problem throughout the world at present. In the future, this issue will further upturn, owing to the rapid industrialization and population growth. Particularly, the rapid growth of textile and dying industries has imposed critical environmental problems, as some of the dye effluents from these industries can pollute the ground water resources and the utilisation of the same creates many toxic and harmful effects on human beings. In this respect, different types of photocatalytic materials *viz.* free standing photocatalysts, doped photocatalysts, dual semiconductors and noble metal deposited photocatalysts have been developed for the treatment and purification of dye-contaminated waste water. Among them, very few have been reported on the basis of physical separation technique by which the photocatalysts can be seperated easilyfrom the reaction medium. The major disadvantage of colloidal photocatalytic system is the complicated separation of catalyst from the reaction medium. To overcome this issue, magnetic separation of photocatalyst has been proposed as a promising solution. The magnetically separable photocatalytic systemes have moreadvantageous over colloidal photocatalytic systems as they do not require filtration or centrifugation for the removal of catalyst from the reaction medium. Hence, the physical separation of a photocatalyst can easily be achieved by using the magnetically separable photocatalysts.

Graphene, a single layer of sp^2-bonded carbon atoms arranged in a two-dimensional (2D) honeycomb structure, possesses high surface area and excellent thermal, mechanical and electrical properties that make it as a good supporting material for inorganic nanoparticles towards various energy and environmental

applications.[1, 2] The combination of graphene with the inorganic nanoparticles liberates new functional hybrid materials, which possesses complementary behaviour between each constituent and thus opens up new opportunities for the enhancement of wider applications.[3, 4] These graphene-based nanocomposites materials not only show significant improvement in electrochemical activity and also lead to the high photocatalytic activity of composites, because the unique surface properties of graphene enable it to accept electrons to impede the recombination of photoinduced electrons and holes, and provides the absorption of dye through π-π conjugation between dyes and aromatic regions of graphene towards environmental remediation applications.[5-7] Although these graphene-based nanocomposites (e.g. rGO-TiO_2, rGO-ZnO, etc.) display excellent performance in the photocatalytic systems, the problems associated with the recovery, reuse and separation of catalysis from the reaction medium still exist after the photodegradation process, because the good dispersive property of these materials caused them to be inconvenient to recycle. Hence, introduction of magnetic nanophotocatalyst materials into the graphene sheets can provide a convenient magnetic separation in order to remove and recycle the magnetic nanocomposite catalysts under an external magnetic field.[8, 9] Recently, magnetite (Fe_3O_4) nanoparticles have attracted much attention because of their low-cost, eco-friendly, simple preparation and show desirable properties of strong super-paramagnetic, electrical conductivity, as well as optical and chemical properties.[10, 11] Hence, they find potential applications in the areas of biosensors,[12] catalysis,[13, 14] supercapacitors[15] and photocatalysis.[16] Few studies showed that the bare Fe_3O_4 nanoparticles are photocatalytically inactive under solar irradiation, owing to the rapid aggregation caused by the high surface area and magnetic interactions between these particles, which lead to the formation of larger Fe_3O_4 particles and hence hinder their

chemical and photocatalytic properties. The incorporation of these Fe_3O_4 nanoparticles into the graphene sheets is a promising solution to overcome this limitation as it prevents the serious agglomeration of magnetite nanoparticles,[17, 18] which leads to high photocatalytic performance under sunlight by the contribution of improved photo-induced charge separation efficiency with in the Fe_3O_4 nanoparticles.[19]

In this investigation, we reported a green, facile and cost-effective method to prepare rGO/Fe_3O_4 nanocomposite materials at room temperature, which is magnetically separable and recyclable. The photocatalytic performance of the prepared rGO/Fe_3O_4 nanocomposite materials were evaluated towards the degradation of a model organic dye, methylene blue (MB). The influence of different content of Fe_3O_4 nanoparticles in magnetically separable (rGO/Fe_3O_4) photocatalysts were studied to optimize the Fe_3O_4 nanoparticles to obtained maximum photodegradation efficiency. The magnetically separable rGO/Fe_3O_4 photocatalysts showed better photocatalytic performance when compared to the controlled samples such as rGO and pristineFe_3O_4 nanoparticles. Moreover, the separated rGO/Fe_3O_4 was reused for several photodegradation experiment cycles to elucidate their sustainability.

2. Experimental Methods

2.1 Materials

Chemical reagents such as sulphuric acid (H_2SO_4, 98%), potassium permanganate ($KMnO_4$, 99.9%), hydrogen peroxide (H_2O_2, 30%), iron (II) sulphate ($FeSO_4.7H_2O$, 99.5%), methylene blue (MB) and ammonium hydroxide (NH_4OH, 25%) were purchased from Systerm and used as such. Graphite flakes were purchased

from Ashbury Inc. All other chemicals used in this work were of analytical grade. Unless otherwise specified, deionized double distilled water was used for all the experiments.

2.2 Preparation of graphene oxide

Graphene oxide (GO) was synthesized from graphite by adopting the simplified Hummer's method.[20] Briefly, 3 g of graphite flakes were oxidatively treated with 400 mL of H_2SO_4 and 18 g of $KMnO_4$ for 5 min under magnetic stirring for the development of graphite oxide. However, to ensure complete oxidation of graphite, the solution was stirred for another 3 days. During the oxidation process, the colour change of the solution from dark purplish-green to dark brown was observed. Then, H_2O_2 solution was added to stop the oxidation process during which, the colour of the solution was changed to bright yellow and this indicated the highly oxidized level of graphite. The obtained graphite oxide was washed 3 times by aqueous solution containing 1 M of HCl and this procedure was repeated until the solution pH became 4–5. At this pH, the graphite oxide was experienced exfoliation, which resulted in thickening of the GO solution and formation of GO gel. Finally, the GO gel was freeze-dried to obtain solid GO.

2.3 Preparation of rGO/Fe_3O_4

The rGO/Fe_3O_4 nanocomposites with different weight ratios of rGO and Fe_3O_4 were prepared by a simple in-situ chemical synthesis method. Typically, 25 mg of GO was dispersed in deionized double distilled (DD) water under stirring which was subjected to sonication for 20 min. Then, 25% of NH_4OH solution was added drop-wise into the GO solution until the pH reached was attained ~11–12.

Further, a desired quantity of $FeSO_4$ solution was slowly added to the above solution containing the GO under magnetic stirring and left overnight at room temperature. The obtained black solution containing rGO/Fe_3O_4 nanocomposite was centrifuged, washed with DD water for 10 min at 4,000 rpm and this procedure was repeated for three times to remove excess NH_4OH present in the solution. Finally the solution was dried in a vacuum oven. The same protocol was followed to prepare Fe_3O_4 nanoparticles in the absence of GO. Meanwhile the rGO was prepared by using the same procedure without adding $FeSO_4$ solution. The weight ratios between the GO and $FeSO_4$ are given in Table 1.

Table 1 Weight ratios between GO and $FeSO_4$ used for the preparation of rGO/Fe_3O_4.

Sample	m_{GO} (mg)	m_{FeSO4} (mg)	Weight Ratio (GO: $FeSO_4$)
G1F2	25	50	1:2
G1F5	25	125	1:5
G1F10	25	250	1:10
G1F20	25	500	1:20
G1	25	-	-
F20	-	500	-

2.4 Characterization techniques

The size, shape and morphology of rGO/Fe_3O_4nanocomposites were analyzed through high resolution transmission electron microscope (HR-TEM). Raman and photoluminescence spectral data were collected using a Renishaw 2000 inVia Raman microscope system with an argon ion laser emitting at 514.5 nm. Siemens-D5000 x-ray diffractiometer with copper Kα radiation (λ = 1.5418 Å) at a scan rate of 0.02 degree/sec was used for XRD analysis. Thermo Scientific Evolution-300 UV-vis

absorption spectrophotometer was employed for absorption studies in the spectral range of 190–900 nm. The magnetization measurements were carried out at room temperature using a Lakeshore-736 vibrating sample magnetometer (VSM) with a maximum magnetic field of 10 kOe.

2.5 Photocatalytic studies

The photocatalytic performance of the prepared rGO/Fe_3O_4 samples were evaluated against methylene blue (MB) dye as a model target organic pollutant under natural sunlight irradiation. The photocatalytic experiments were performed on bright sunny days from 9 a.m. to 2 p.m. All the prepared photocatalyst materials (2 mg) were separately dispersed in 12 mL of MB solution (10 mg/L) under stirring and left overnight (12 h) at room temperature in order study the adsorption behaviour. Prior to the sunlight irradiation, the MB solution was stirred for 1 h in dark thereby allow the system to attain an adsorption-desorption equilibrium between photocatalyst and MB molecules. At given time intervals of irradiation, 2 mL of irradiated MB dye solution was periodically withdrawn and at the end of the experiment the photocatalyst was removed from the reaction solution by magnetic separation using a permanent magnet. The equilibrium concentration of MB dye in the reaction solution for each sample was determined by a UV-visible absorption spectrophotometer by measuring the absorbance intensity at 662 nm during the photocatalytic degradation process. To study the sustainability of photocatalysts, the rGO/Fe_3O_4 was collected by applying a magnetic field and washed with DI water before re-dispersed into fresh MB solution for the next cycle.

The photodegradation rate and MB dye removal efficiency under natural sunlight irradiation, in the presence of different photocatalysts were calculated by the following equations.

Photodegradation rate = $\frac{C_t}{C_0}$ ------- (Eqn. 1)

Dye removal efficiency = $\left(1 - \frac{C_t}{C_0}\right) \times 100\ \%$ ------- (Eqn. 2)

where, C_0 represents the initial concentration of MB and C_t is the concentration of MB at a reaction time 't'.

3. Results and discussion

3.1. Morphological characterization of rGO/Fe_3O_4 nanocomposites

The TEM images of Fe_3O_4 and rGO/Fe_3O_4 nanocomposite materials before and after the 8 cycles of photocatalytic experiments are shown in Fig. 1 and Figure 2(a-e), respectively The TEM images clearly indicate that the Fe_3O_4 nanoparticles are uniformly embedded on the surface of rGO sheets in all the nanocomposite materials and no significant change in the morphology of rGO/Fe_3O_4 nanocomposite is observed before and after the photocatalytic studies (Fig. 1 and 2). The lowering tendency agglomeration of Fe_3O_4 and restacking of rGO sheets are vital in determine the photocatalytic activity of rGO/Fe_3O_4 nanocomposite. The lattice resolved TEM image of rGO/Fe_3O_4 nanocomposite reveals the presence of clear atomic lattice-fringes of Fe_3O_4 nanoparticles on the surface of rGO sheets (Fig. 2f). The estimated lattice-fringe or fringe values of magnetic Fe_3O_4 nanoparticles are 2.533 Å and 1.643 Å, which can be respectively indexed to the (3 1 1) plane (2.530 Å) and (5 1 1) plane (1.614 Å) which is compatible with the XRD observation. The increase in the concentration of $FeSO_4$ nanoparticles during the preparation of nanocomposite showed increase in the particles size of Fe_3O_4 in the order of G1F2 < G1F5 < G1F10

< G1F20 (Fig. 1(b–f)) which disclose that the aggregation tendency of Fe_3O_4 nanoparticles in the rGO/Fe_3O_4 nanocomposite becomes more and more when increasing the $FeSO_4$ precursor concentration. Among the different nanocomposite materials, the G1F20 showed the maximum aggregation of Fe_3O_4 nanoparticles (Fig. 1(f)), while the G1F2 exhibited a good distribution of Fe_3O_4 nanoparticles on the surface of rGO sheets (Fig. 1(c)).

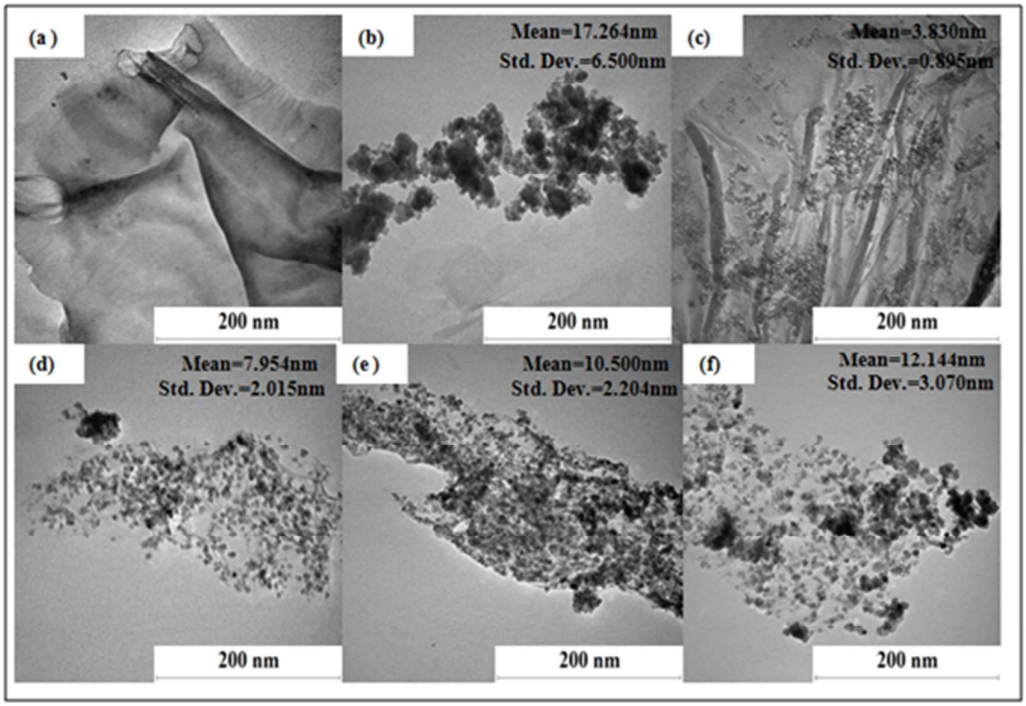

Fig. 1 TEM images of G1 (a), F20 (b), G1F2 (c), G1F5 (d), G1F10 (e) and G1F20 (f) before the photocatalytic process.

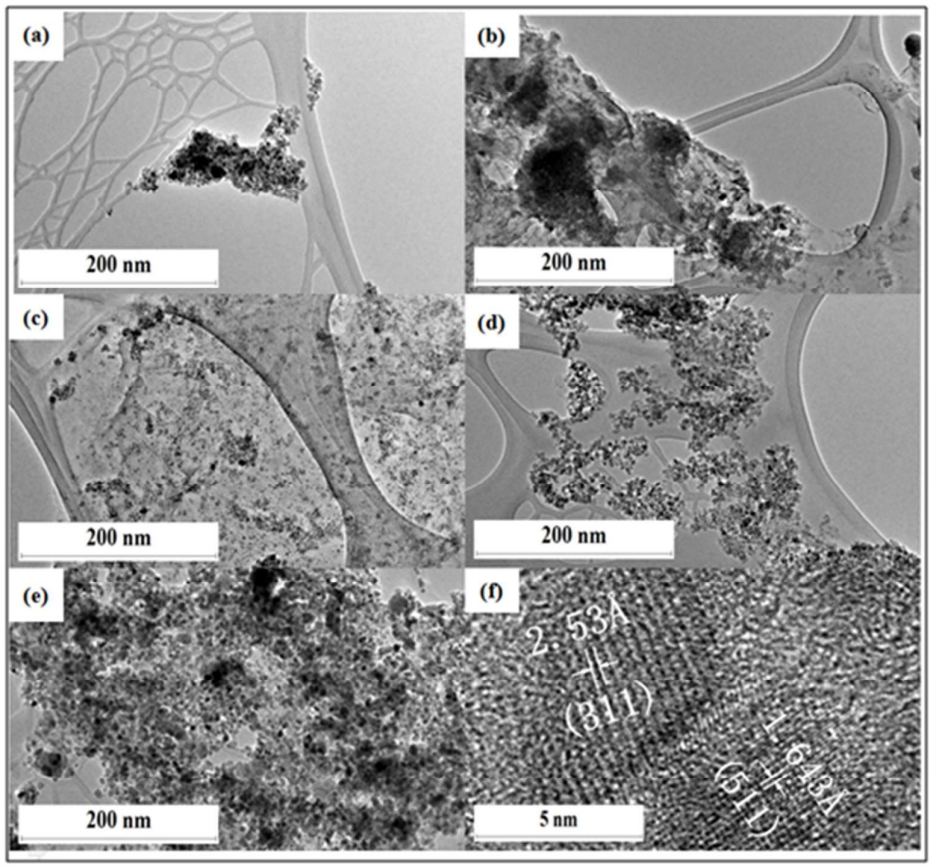

Fig. 2 HR-TEM images of F20 (a), G1F2 (b), G1F5(c), G1F10 (d) and G1F20 Fe_3O_4/rGO (e) after 8 cycles of the photocatalytic process and G1F20 (f) at a higher magnification.

3.2. XRD studies of Fe_3O_4/rGO nanocomposites

Fig. 3 portrays the representative XRD patterns of G1, F20 and rGO/Fe_3O_4 nanocomposites, which coincides with the result from HRTEM image (Fig. 2(f)) and ensure the formation of Fe_3O_4 crystallites in the nanocomposites. The XRD pattern of F20 (Fig. 3(e)) displayed a series of diffraction peaks at 2θ = 30.2°, 35.6°, 43.3°, 53.7°, 57.3°, and 62.8°, corresponding to the reflection from (2 2 0), (3 1 1), (4 0 0), (4 2 2), (5 1 1), and (4 4 0) crystal planes of the cubic spinel structure of magnetite Fe_3O_4. A sharp peak observed in G1 (Fig. 3(a)) at 2θ = 10.8° is assigned to the (0 0 1)

reflection of GO, which indicates that GO was incompletely reduced to rGO. For the sample rGO/Fe_3O_4 containing Fe^{2+} ions, this (0 0 1) plane was absent, and hence suggests that Fe^{2+} plays important role as reducing agent in the redox reaction of nanocomposite fabrication. For sample G1F2, this sharp XRD line was observed and meanwhile the diffraction peaks for Fe_3O_4 were not detected, owing to the low amount of Fe^{2+} ions in nanocomposite resulted the partially reduction of GO. However, when increased the content of Fe_3O_4, the five typical characteristic diffraction peaks of Fe_3O_4 and the disappearance of graphitic peak were clearly observed for G1F5 and G1F10 (Fig. 3(c-d)), which can be ascribed to the formation of van der Waals and π- π stacking interactions between rGO sheets prevented by Fe_3O_4 nanoparticles. [21]

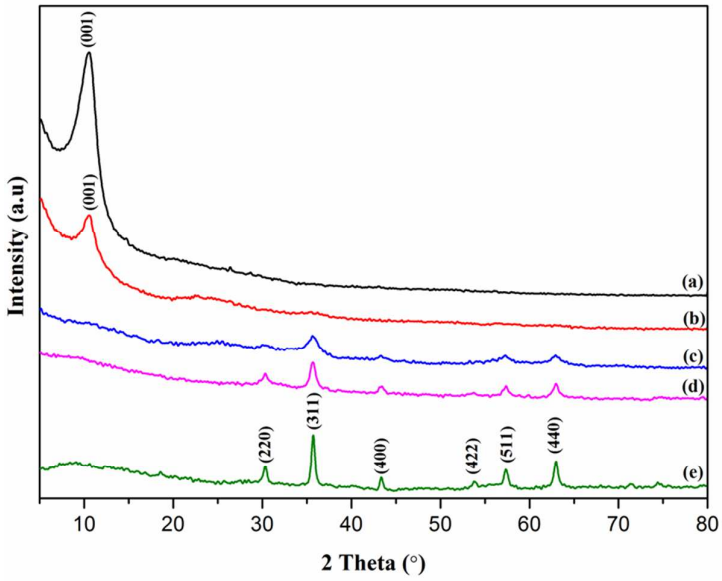

Fig. 3 XRD patterns of G1 (a), G1F2 (b), G1F5 (c), G1F10 (d), and (e) F20.

3.3. Raman spectral studies of Fe_3O_4/rGO nanocomposites

Raman spectroscopy is an excellent tool to investigate the ordered and disordered crystal structures of carbonaceous materials, *viz.* graphene, graphene oxide

and reduced graphene oxide. Raman spectra of GO, G1 and rGO/Fe_3O_4 photocatalyst materials were recorded and are presented in Fig. 4. Fig. 4(Inset) shows the existence of D band around 1,350 cm^{-1} which can be ascribed to the sp^3 defects and the G band around 1,580 cm^{-1} is related to the in-plane vibration of sp^2 carbon atoms in a 2D hexagonal lattice of GO and rGO. The observed position and intensity of D and G bands highly influence the structural transformation in carbonaceous materials. The I_D/I_G ratio of rGO/Fe_3O_4 nanocomposites (0.92–1.15) show remarkable increases (Fig. 4(c–f)) when compared to that of GO (0.91), due to the higher amount of Fe_3O_4 in the nanocomposite. The relatively high intensity of D band when compared to the G band of rGO/Fe_3O_4, indicating the presence of localized sp^3 defects within sp^2 clusters during functionalization process of exfoliated GO.[22, 23] Besides, the characteristic Raman peak around 670 cm^{-1} suggests the presence of magnetite (Fe_3O_4) (Fig. 4(c–g)). It is known from the earlier report that the observed broad peak at ~670 cm^{-1} is due to the presence of magnetite nanoparticles in the rGO/Fe_3O_4 nanocomposites.[24]

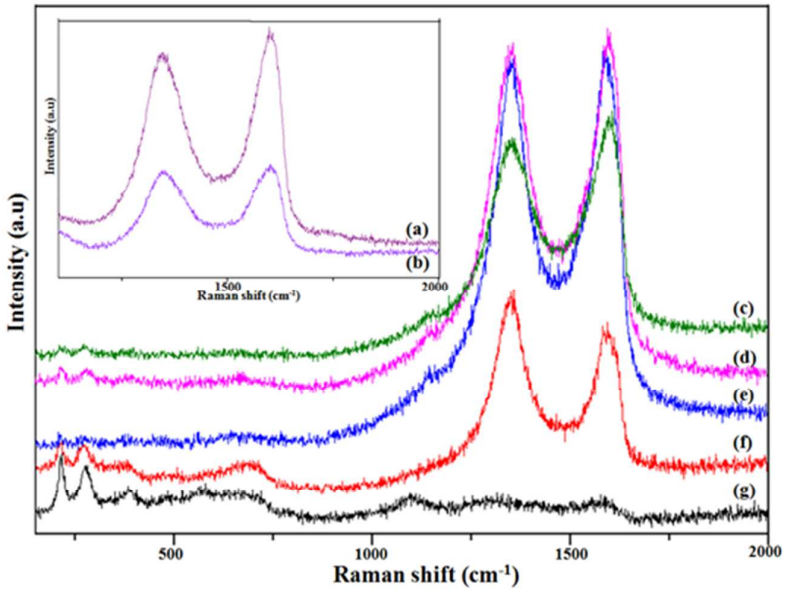

Fig. 4 Raman spectra for the GO (a), G1 (b), G1F2 (c), G1F5 (d), G1F10 (e), G1F20 (f) and F20 (g).

3.4. Magnetic behaviour of Fe_3O_4/rGO nanocomposites

Studying the magnetic behaviour of the prepared magnetically separable rGO/Fe_3O_4 nanocomposites is very essential. In this respect, VSM analysis was carried out at room temperature for both the bare Fe_3O_4 nanoparticles and rGO/Fe_3O_4 nanocomposites and the results are shown in Fig. 5. The bare Fe_3O_4 nanoparticles and rGO/Fe_3O_4 nanocomposites showed typical S-like curve magnetization hysteresis loops with no coercivity, inferring that they exhibit super-paramagnetism and the magnetization behaviour was removed in the absence of the applied magnetic field. The saturation magnetization (Ms) of rGO/Fe_3O_4 nanocomposites was increased from 1.63 emu/g to 30.30 emu/g, while increasing the content of Fe_3O_4 nanoparticles in the rGO sheets. The saturated magnetization value was observed for pristine Fe_3O_4 nanoparticles (58.70 emu/g), which was higher than that of magnetic rGO/Fe_3O_4 nanocomposites and this can be attributed to the presence of graphene in the nanocomposites.[25]

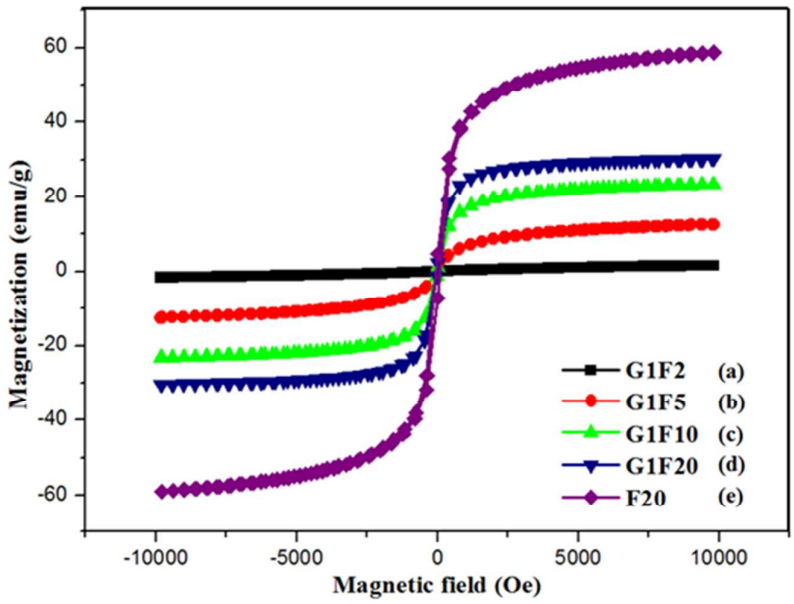

Fig. 5 VSM magnetization curves of G1F2 (a), G1F5 (b), G1F10 (c), G1F20 (d) and F20 (e).

3.5. Photoluminescence studies of rGO/Fe_3O_4 nanocomposites

Photoluminescence (PL) technique is used to study the electronic and optical properties inlcuding the migration, transfer and recombiantion of electron-hole pair of photoinduced semiconductor. Fig. 6 represents the room temperature PL spectra of rGO, rGO/Fe_3O_4 nanocomposites and Fe_3O_4. It is observed from the PL spectra that the rGO and rGO/Fe_3O_4 nanocomposites have exhibited lower PL intensity than that of the bare Fe_3O_4 nanoparticles. Fe_3O_4 is an indirect band gap semiconductor with a narrow optical gap value of 1.4 eV.[26] This narrowness value arises from the d orbitals suggested that Fe_3O_4 exhibits high electrical conductivity with almost metallic nature at room temperature, but with the low charge carriers (electron and hole) mobility in Fe_3O_4, may lead to an increase in electron-hole of recombination. Therefore, the higher PL intensity of the bare Fe_3O_4 is due to the recombination of excited electrons and holes whereas, the lower PL emission intensity of rGO and Fe_3O_4/rGO nanocomposites is due to the lower charge recombination rates. This disclose that graphene have the tendency to greatly influence the PL intensities of rGO/Fe_3O_4 nanocomposites, owing to the 2D hexagonal π-conjugation structure and excellent electronic conductivity of graphene. The high charge mobility of graphene act as electron acceptor for the photo-excited electrons from Fe_3O_4, leading to low charge recombination rate.[27, 28 29] Among the prepared nanocomposites and rGO, the G1F2 has the lowest PL intensity, which indicates that the G1F2 efficiently suppresses the electron-hole pair recombination and promotes the charge separation and these are highly beneficial for photocatalytic applications. The synergistic effect[30] between graphene and Fe_3O_4 nanoparticles in the G1F2 nanocomposite allows graphene to capture or trap the the photo-induced electrons from conduction band of Fe_3O_4 through the extended π-conjugation carbon network and consequently restricted the

flash recombination of electron-hole pair. Therefore, G1F2 is expected to show higher photocatalytic activity when compared to the other nanocomposites.[31] However, further increasing the Fe_3O_4 content in the rGO/Fe_3O_4 nanocomposite results in a higher PL intensity. The Fe_3O_4 nanoparticles possess large surface energies and hence they tend to aggregate to minimize the surface energies. Thus, excess content of Fe_3O_4 nanoparticles in the rGO/Fe_3O_4 nanocomposite may lead to aggregation of nanoparticles that results in larger particles.[32] Consequently, increasing the amount of Fe_3O_4 nanoparticles in the rGO/Fe_3O_4 nanocomposite introduce new charge recombination centres for photoinduced charge separation and as a consequence they minimize the photocatalytic efficiency.

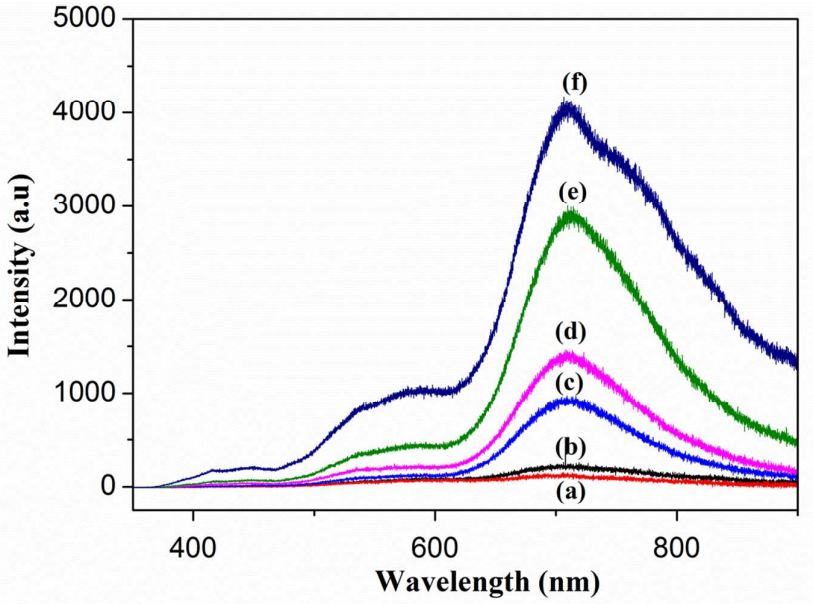

Fig. 6 Room temperature photoluminescence (PL) spectra of G1F2 (a), rGO (b), G1F5 (c), G1F10 (d), G1F20 (e) and F20 (f).

3.6. Photocatalytic activity of magnetically separable rGO/Fe_3O_4 nanocomposites towards the degradation of methylene blue

The photocatalytic performance of the prepared photocatalytic materials *viz.* rGO, Fe_3O_4 and magnetically separable rGO/Fe_3O_4 nanocomposites was separately evaluated towards the degradation of a model dye pollutant, methylene blue (MB) under natural sunlight irradiation of 5 h. The results of the photodegradation study are shown in Fig. 7a. During photocatalytic experiments, the bare Fe_3O_4 nanoparticles showed only 57 % of photodegradation even up to 5 h of sunlight irradiation (Fig. 7a). The poor photocatalytic performance of the bare Fe_3O_4 nanoparticles can be ascribed to the aggregation caused by the high surface area Fe_3O_4 nanoparticles and magnetic interactions between these particles lead to the formation of larger size particles.[33] Interestingly, a maximum photodegradation of MB was observed at 1 h light irradiation when Fe_3O_4 nanoparticles incorporated reduced graphene oxide sheets was used as a photocatalyst. To optimize the Fe_3O_4 content for maximum photodegradation of MB dye, the photocatalytic experiments were carried out with different compositions of rGO and Fe_3O_4. Among the photocatalysts, the G1F2, exhibited excellent photocatalytic activity and almost 89 % of MB was decolourized upon 30 min and 100 % after 1 h light irradiation. The GIF5, GIF10 and GIF 20 were showed 100 % degradation of MB after 2 h of irradiation. Meanwhile, the bare Fe_3O_4 nanoparticles photocatalyst could achieve only 57 % MB dye removal efficiency. The maximum photocatalytic activity exhibited by the rGO/Fe_3O_4 nanocomposite photocatalysts is due to the emergence of synergistic effect in the rGO/Fe_3O_4 during photocatalytic reaction i.e. efficient photogenerated charge transfer from Fe_3O_4 to graphene sheets which facilitates increased electron-hole pair separation and as a consequence better photocatalytic performance was achieved.

Further to understand the enhanced photocatalytic performance of the rGO/Fe_3O_4 nanocomposites, the MB solution was continuously stirred with

photocatalysts overnight (12 h) and their results are shown in Fig. 7b. The rGO and GIF2 showed maximum adsorption of ~86 and ~84 %, respectively. Further increasing the Fe_3O_4 content in the nanocomposite leads to decrease the adsorption of MB. The shadowed area in the Fig. 7a follows the similar trend to the adsorption behaviour of the photocatalysts. The enhanced MB dye adsorptivity of rGO/Fe_3O_4 photocatalysts is due to the presence of large phenyl ring structure of graphene[34, 35] in the nanocomposites. Moreover, graphene is a 2D crystalline structure and has a large surface area, superior electrical conductivity and unique transport property, make it a great electron-transport material in the process of photocatalysis. When Fe_3O_4 nanoparticles are anchored on the surface of graphene sheets, the graphene provides more adsorption sites and photocatalytic reaction centres for the MB dye molecules through the π-π conjugation and electrostatic attraction between the MB dye and the aromatic region of graphene sheets.[36, 37] These highly exposed surface active reaction sites is beneficial to promote the generation of hydroxyl radicals for MB adsorption by redox reaction within the active sites ($Fe^{2+/}Fe^{3+}$). Additionally, the strong Fe-O-C interaction of rGO/Fe_3O_4 between the delocalized unpaired π electrons from π-conjugated carbon network on graphene's basal plane facilities the electron-transfer between rGO sheets and iron centres.[38] Notably, the photocatalytic activity is highly depends on the concentration of photogenerated of charge carriers during the reaction.[39] Therefore, the strong attachment of Fe_3O_4 on electron carries of rGO sheets gives rise to a enhanced migration of photoexcited electrons from the conduction band of Fe_3O_4 to rGO sheets. The fast electron-transfer kinetic of rGO/Fe_3O_4 attempts to improve the interfacial charge transfer process[40] leading to the enhanced photocatalytic activity. On the other hand, the strong anisotropic dipolar interactions of Fe_3O_4 in aqueous phase[41] are likely to diminish or restrict their catalytic activity,

and thus the Fe_3O_4 nanoparticles are prone to aggregate into larger Fe_3O_4 particles (Fig. 1(b)), leading to the decreased MB decolourization efficiency.

The sustainability of a photocatalyst is one of the most important requirements for successful practical applications. In this respect, the reusability of rGO and rGO/Fe_3O_4 photocatalyst was investigated by using the same photocatalyst for 8 sets of experiments with fresh MB solution at each experiment and keeping all other experimental parameters as constant. After each photodegradation experiment, the photocatalyst was removed from the photolysis cell by using external magnetic field and washed with high pure DI water to remove the presence of any MB associated organic impurities. The magnetic separation technique facilitates an easy and convenient way to remove or recycle the photocatalyst. This can be achieved by placing a magnet close to the sample bottle and as a consequence, the rGO/Fe_3O_4 photocatalyst moves towards external magnetic field and attracted to the side of the bottle, leaving behind a clear reaction solution (Fig. 7(d)). Therefore, the rGO/Fe_3O_4 can be easily repeated and recycled after photocatalytic process. The MB dye molecules could be effectively photodecomposed in each experimental cycle and no significant change in the photocatalytic activity of the G1F2 nanocomposite was observed during the repeated photocatalytic experimental cycles (Fig. 7c).

Among the different photocatalysts, the G1F2 nanocomposite exhibited most good stability during photocatalytic degradation of MB dye and hence they can be applied as a recyclable photocatalyst. The lower the content of Fe_3O_4 nanoparticles in the nanocomposites, smaller the particle size with high surface area without heavy aggregation of Fe_3O_4 nanoparticles and therefore they can offer excellent decolourization activity. Hence, the G1F2 contains the lowest amount of Fe_3O_4

nanoparticles have the smaller particles size with high specific surface area, that offers number of active sites for adsorption and subsequent desorption of MB molecules in the nanocomposite, favours the facile transport of photoexcited electrons to reach at the surface reaction sites more easily[42] and thereby efficiently inhibited the recombination of photo-induced electron-hole pairs during electron-transfer process. Thus, the higher photocatalytic activity and sustainability of this magnetically separable rGO/Fe_3O_4 nanocomposite is more beneficial for industrial waste water treatment process.

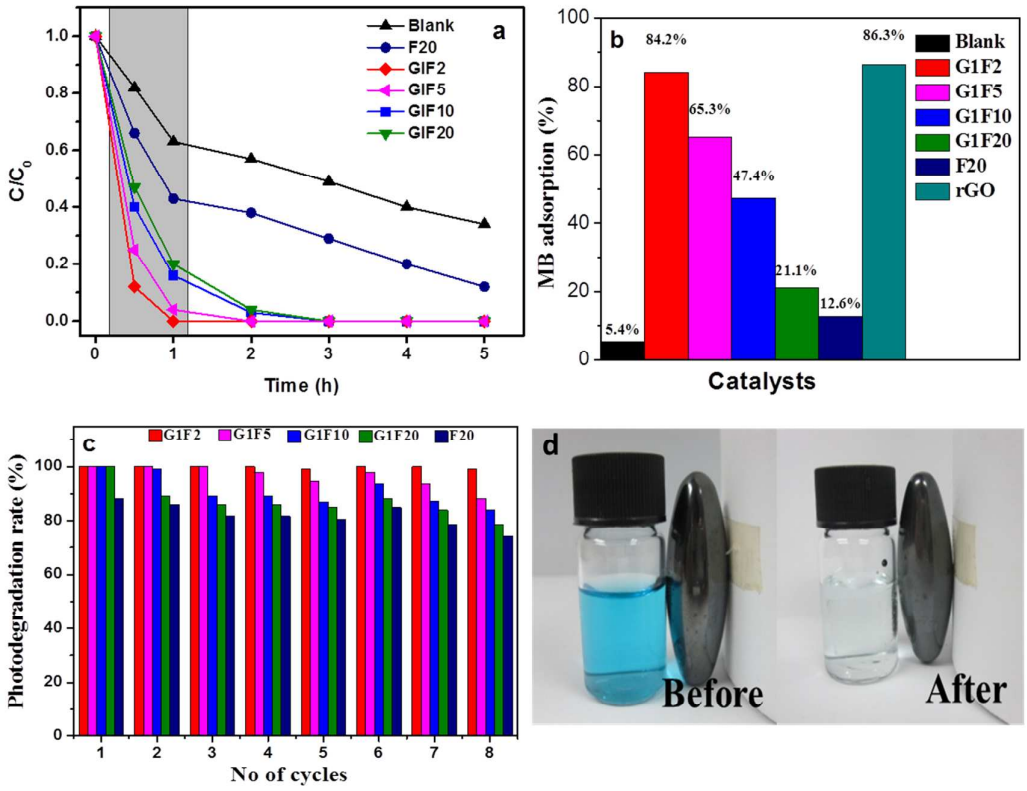

Fig. 7. Photocatalytic degradation of MB in the presence of different photocatalysts under sunlight irradiation (a). Adsorption of MB by different catalysts after 12 h stirring. (b). Photodegradation efficiency (%) of MB solution for 8 cycles in the presence of rGO/Fe_3O_4 nanocomposites and Fe_3O_4 (c). Photographic images of MB before and after degradation by rGO/Fe_3O_4 and recovery by applying an external magnet (d).

The schematic representation of MB degradation in the presence of magnetically separable rGO/Fe_3O_4 photocatalyst is shown in Fig. 8. Upon light irradiation, the Fe_3O_4 present on the rGO sheet surface undergoes charge separation that leads to promotion of valence band (VB) electrons into the conduction band (CB), leaving a hole in the VB (Eqn. (1)), whereas the MB molecules excited to cationic MB radicals (MB^*) (Eqn. (2)). These photogenerated electrons in the conduction band instantaneously transferred to rGO sheets (Eqn. (3)) and consequently captured by dissolved O_2 to generate reactive oxidation species, such as ·OH and $O^{2\bullet-}$ (Eqn. (4)). On the other hand, the photoinduced holes are crucial for oxidation process and it effectively oxidizes the adsorbents, usually it can react with adsorbed H_2O/OH^- to form strong hydroxyl radicals (·OH) (Eqn. (5)). Finally, these ·OH radicals oxidize the MB molecules adsorbed to CO_2 and H_2O (Eqn. (6)) [43] *via* the π-π stacking/electrostatic interactions on the active sites of rGO/Fe_3O_4 nanocomposites.

$$Fe_3O_4 + h\nu \longrightarrow Fe_3O_4\,(e^- + h^+) \quad (1)$$

$$MB + h\nu \longrightarrow MB^* \quad (2)$$

$$Fe_3O_4\,(e^-) + \text{Graphene} \longrightarrow Fe_3O_4 + \text{Graphene}\,(e^-) \quad (3)$$

$$\text{Graphene}\,(e^-) + O_2 \longrightarrow \text{Graphene} + O^{2\bullet-} \quad (4)$$

$$Fe_3O_4\,(h^+) + OH^- \longrightarrow Fe_3O_4 + {\cdot}OH \quad (5)$$

$$MB^* + {\cdot}OH \longrightarrow CO_2 + H_2O \quad (6)$$

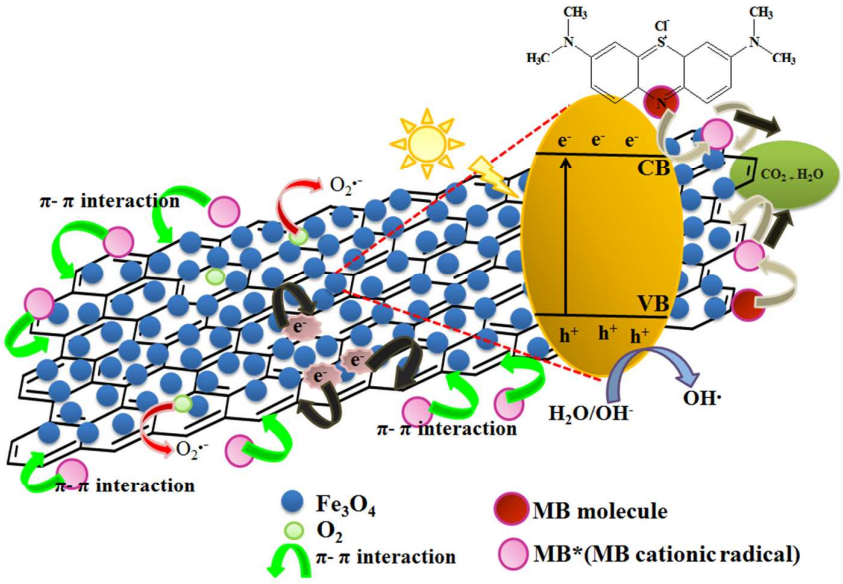

Fig. 8 Schematic representation of photocatalytic degradation of MB in the rGO/Fe_3O_4 nanocomposites under natural sunlight irradiation.

4. Conclusion

We reported the preparation of photocatalysts based on magnetically separable rGO/Fe_3O_4 nanocomposite materials through a simple, eco-friendly and cost-effective approach at room temperature. The obtained nanocomposite materials were characterized by various suitable techniques such as HRTEM, XRD, VSM, Raman, PL and UV-vis spectrophotometer. The XRD pattern indicated the formation of Fe_3O_4-rGO nanocomposites and the HRTEM showed that the Fe_3O_4 nanoparticles with an average size of 10 nm were incorporated into the rGO sheets. The super-paramagnetic property of the rGO/Fe_3O_4 nanocomposite materials were revealed through the VSM analysis. This super-paramagnetic behaviour of the rGO/Fe_3O_4 nanocomposites is more advantageous to design a solid–solution system for photocatalytic applications as it facilitates the simple physical separation of the catalyst from the solution in contrast to the other colloidal photocatalyst system. The

rGO/Fe_3O_4 exhibited excellent adsorption behaviour and enhanced photocatalytic performances towards the degradation of methylene blue (MB) dye. This enhanced photocatalytic activity could be attributed to the emergence of synergistic effect between the rGO and Fe_3O_4 and as a consequence of the reduced charge recombination. The rGO/Fe_3O_4 possessed good sustainability even after eight cycles of MB photodegardation and moreover the morphology of the photocatalyst was unaffected. These features of magnetically separable rGO/Fe_3O_4 make it a promising and recyclable photocatalyst for many environmental remediation applications.

Acknowledgements

This work was financially supported by Exploratory Research Grant Scheme (ER016–2011A), Fundamental Research Grant Scheme (UKM-FST-07-FRGS0233–2010), and High Impact Research Grant from the Ministry of Higher Education of Malaysia (UM.C/625/1/HIR/MOHE/05).

References

1. G. Williams, B. Seger and P. V. Kamat, *J. Am. Chem. Soc.*, 2008, **2**, 1487-1491.
2. X. M. Chen, G. H. Wu, Y. Q. Jiang, Y. R. Wang and X. Chen, *Analyst*, 2011, **136**, 4631-4640.
3. H. T. Hu, X. B. Wang, F. M. Liu, J. C. Wang and C. H. Xu, *Synth. Met.*, 2011, **161**, 404-410.
4. J. F. Shen, B. Yan, M. Shi, H. W. Ma, N. Li and M. X. Ye, *J. Mater. Chem.*, 2011, **21**, 3415-3421.
5. G. Z. Liao, S. Chen, X. Quan, H. T. Yu and H. M. Zhao, *J. Mater. Chem.*, 2012, **22**, 2721-2726.
6. M. S. A. Sher Shah, A. R. Park, K. Zhang, J. H. Park and P. J. Yoo, *ACS Appl. Mater. & Interfaces*, 2012, **4**, 3893-3901.
7. J. Zhang, Z. Xiong and X. Zhao, *J. Mater. Chem.*, 2011, **21**, 3634-3640.
8. X. Y. Li, X. Wang, S. Y. Song, D. P. Liu and H. J. Zhang, *Chem. Eur. J.*, 2012, **18**, 7601-7607.

9. Z. J. Luo, H. J. Tang, L. L. Qu, T. T. Han and X. Y. Wu, *Cryst. Eng. Comm*, **14**, 5710-5713.
10. H. X. Wu, G. Gao, X. J. Zhou, Y.Zhang and S. W. Guo, *Cryst. Eng. Comm*, 2012, **14**, 499-504.
11. D. M. Fouad and M. B. Mohamed, *J. Nanotechnol.*, 2011, DOI: 10.1155/2011/416060, 1-7.
12. C.M.Yu, L. L. Gou, X. H. Zhou, N. Bao and H. Y. Gu, *Electrochim. Acta*, 2011, **56**, 9056-9063.
13. E. M. Rodríguez, G. Fernández, P. M. Álvarez, R. Hernández and F. J. Beltrán, *Appl. Catal., B*, 2011, **102**, 572-583.
14. K. Wang, L. X. Yu, S.Yin, H. N. Li and H. M. Li, *Pure Appl. Chem.*, 2009, **81**, 2327-2335.
15. W. H. Shi, J. X. Zhu, D. H. Sim, Y. Y. Tay, Z. Y. Lu, X. J. Zhang, Y. Sharma, M. Srinivasan, H. Zhang, H. H. Hng and Q. Y. Yan, *J. Mater. Chem.*, 2011, **21**, 3422-3427.
16. Y.Fu and X. Wang, *Ind. Eng. Chem. Res.*, 2011, **50**, 7210–7218.
17. H. K. He and C. Gao, *ACS Applied Mater. & Interfaces*, 2011, **2**, 3201-3210.
18. J. J. Liang, Y. F. Xu, D. Sui, L. Zhang, Y. Huang, Y. F. Ma, F. F. Li and Y. S. Chen, *J. Phys. Chem. C*, 2010, **114**, 17465-17471.
19. Y. S. Fu, H. Q. Chen, X. Q. Sun and X. Wang, *Appl. Catal., B*, 2012, **111-112**, 280-287.
20. H. N. Lim, N. M. Huang, S. S. Lim, I. Harrison and C. H. Chia, *Int. J. Nanomed.* , 2011, **6**, 1817–1823.
21. X. W. Wang, H. W. Tan, Y. Yang, H. Wang, S. M. Wang, W. T. Zheng and Y. C. Liu, *J. Alloys Compd.*, 2012, **524**, 5-12.
22. M. Sathish, T. Tomai and I.Honma, *J. Power Sources*, 2012, **217**, 85-91.
23. V. Chandra, J. S. Park, Y. Chun, J. W. Lee, I. C. Hwang and K. S. Kim, *ACS Nano*, 2010, **4**, 3979-3986.
24. K. Ritter, M. S. Odziemkowski and R. W. Gillham, *J. Contam. Hydrol.*, 2002, **55**, 87-111.
25. L. L. Ren, S. Huang, W. Fan and T. X. Liu, *Appl. Surf. Sci.*, 2011, **258**, 1132-1138.
26. D. Beydoun, R. Amal, G. K.-C. Low and S. McEvoy, *J. Phys. Chem. B*, 2000, **104**, 4387-4396.
27. X. J. Liu, L. K. Pan, T. Lv, G. Zhu, T. Lu, Z. Sun and C. Q. Sun, *RSC Adv.*, 2011, **1**, 1245-1249.
28. Y. Zhang, G. Li, H. Lu, Q. Lv and Z. Sun, *RSC Adv.*, 2014, **4**, 7594-7600.
29. D. K. Padhi and K. Parida, *J. Mater. Chem. A*, 2014, **2,** 10300–10312.
30. L. Zhou, Y. Shao, J. Liu, Z. Ye, H. Zhang, J. Ma, Y. Jia, W. Gao and Y. Li, *ACS Appl. Mater. & Interfaces*, 2014, **6**, 7275-7285.
31. Y. Fu and X. Wang, *Ind. Eng. Chem. Res.*, 2011, **50**, 7210-7218.
32. M. Gao, W. Li, J. Dong, Z. Zhang and B. Yang, *World J. Condens. Matter Phys.*, 2011, **1**, 49.
33. W. Wu, Q. G. He and C. Z. Jiang, *Nanoscale Res. Lett.*, 2008, **3**, 397-415.

34. Y. Matsumoto, M. Koinuma, S. Ida, S. Hayami, T. Taniguchi, K. Hatakeyama, H. Tateishi, Y. Watanabe and S. Amano, *J. Phys. Chem. C*, 2011, **115**, 19280-19286.
35. J. C. Qu, C. L. Ren, Y. L. Dong, Y. P. Chang, M. Zhou and X. G. Chen, *Chem. Eng. J.*, 2012, **211–212**, 412-420.
36. T. G. Xu, L. W. Zhang, H. Y. Cheng and Y. F. Zhu, *Appl. Catal., B*, 2011, **101**, 382-387.
37. Y. S. Fu, P. Xiong, H. Q. Chen, X. Q. Sun and X. Wang, *Ind. Eng. Chem. Res.*, 2012, **51**, 725-731.
38. K. Jasuja, J. Linn, S. Melton and V. Berry, *J. Phys. Chem. Lett.*, 2010, **1**, 1853-1860.
39. A. Mukherji, B. Seger, G. Q. Lu and L. Wang, *ACS Nano*, 2011, **5**, 3483-3492.
40. S. Saha, J. Wang and A. Pal, *Sep. Purif. Technol.*, 2012, **89**, 147-159.
41. J. Deng, X. Wen and Q. Wang, *Mater. Res. Bull.*, 2012, **47**, 3369-3376.
42. K. Parida, K. Reddy, S. Martha, D. Das and N. Biswal, *Int. J. Hydrogen Energy*, 2010, **35**, 12161-12168.
43. T. Harifi and M. Montazer, *Appl. Catal., A*, 2014, **473**, 104-115.

Conflict of Interests

The author(s) declare(s) that there is no conflict of interests regarding the publication of this research article.